International Journal of ChemTech Research
CODEN (USA): IJCRGG ISSN: 0974-4290
Vol.7, No.3, pp 1351-1357, 2014-2015

ICONN 2015 [5th -7th Feb 2015]
International Conference on Nanoscience and Nanotechnology-2015
SRM University, Chennai, India

Investigations of optical, structural, and Magnetic properties of Ce–Mn dual-doped ZnO

J. Arul Mary[1] and J. Judith Vijaya[2]*

[1,2]Catalysis and Nanomaterials Research Laboratory, Dept of Chemistry, Loyola College, Chennai, India.

Abstract : A systematic investigation on the synthesis, characterization, optical and magnetic properties of co doped ZnO nanoparticles has been reported. Nanoparticles of (($Zn_{1-2x}Ce_xMn_x$) O (x = 0.00, 0.01, 0.02, 0.03, 0.04, and 0.05)) were synthesized using microwave-assisted combustion method. Structural, optical and magnetic properties of the samples were investigated by X-ray diffraction (XRD), scanning electron microscopy (SEM), energy dispersive X-ray spectroscopy (EDX), diffuse reflectance spectroscopy (DRS) and photoluminescence spectroscopy (PL). The observed shift in the XRD peak position, and the change in peak intensity, confirmed the substitution of dopants into ZnO lattice. The synthesized nanoparticles had different microstructure without changing a hexagonal wurtzite structure. The average crystal size was decreased from 40 nm to 10 nm. The energy dispersive X-ray spectra confirmed the presence of Ce and Mn in ZnO system and the weight percentage was nearly equal to their nominal stoichiometry. DRS measurements showed a decrease in the energy gap with increasing dopants content. The observed luminescence in the green, violet and blue regions strongly depends on the doping elements owing to the different oxygen vacancy, zinc interstitial, and surface morphology. Our results demonstrate that the Mn ions doping concentration play an important role in enhancing the ferromagnetic properties of Ce–Mn dual doped ZnO nanoparticles at room temperature.
Keywords: optical, structural, and Magnetic properties.Ce–Mn dual-doped ZnO.

Introduction

In the last decade, nanosized semiconductor composites represent the accelerated interests for scientific and industrial applications in optical, structural, thermal, bio-medical and electronic devices, photocatalysts, photosensors, electro-photoluminescent displays, solar cells etc[1,2].

Among the metal oxides, ZnO is the preferred wide band gap materials, which has many desirable properties, such as, availability in different shape and size, large exciton binding energy (60 meV), direct wide band gap (3.37 eV), and transparency in the visible region, higher chemical stability, operation at much higher temperatures[3]. Mn-doped ZnO nanostructures have captivated the compelling interest as Mn has the topmost magnetic moment and the first half of the d band is fully occupied[4], creating a stable fully polarized state.

The Ce doped ZnO nanomaterials presented the adaptable properties and much deliberation has been directed to examine the possible applications in various technologies[4,5]. In our work, the dual dopants Ce and

Mn into ZnO nanostructures are fabricated for attaining the desired alteration in the structural, optical and magnetic properties. Microwave combustion is of higher interest, because of immediate high temperatures at the reaction sites, lessened reaction times, reduced energy utilization and greater product yields. Hence, the microwave induced combustion method is a clean and swift method for the production of dual doped ZnO nanoparticles without involving the complicated treatments and expensive materials[6]. To the best of our literature knowledge, we have made the first investigation by dual doping Ce, Mn into ZnO through microwave combustion method. Therefore, in the present investigation, nanoparticles are synthesized and the influence of Ce and Mn concentrations on the structural, optical and morphological properties have been studied and discussed in detail.

Experimental Part

Procedure

All the chemicals employed in this investigation were of analytical grade procured from Merck, India and were used as acquired without further refinement. Zinc nitrate ($Zn(NO_3)_2 \cdot 6H_2O$, 98%), cerium nitrate ($Ce(NO_3)_2 \cdot 6H_2O$, 98%), manganese nitrate ($Mn(NO_3)_2.4H_2O$, 98%) and urea as a fuel were applied in this method. ZnO samples were prepared with the addition of manganese and cerium of varied molar ratios to zinc oxide. The precursor mixture in urea is dissolved in de-ionized water by operating the magnetic stirrer for 30 min and the mixture is drained into a crucible. And, then the crucible is located in a microwave oven working at 800 W for 8 min till the precursor solution mixture decomposes. When the solution arrive the point of spontaneous combustion, it commences with the release of heat by burning and turns into a solid powder. It is the dried in an oven at 100 ºC for 1 h and annealed at 600ºC for 2 h.

Materials characterization

Structural characterization of pure and Ce, Mn dual doped ZnO was performed using a Rigaku Ultima IV high resolution X-ray diffractometer (XRD) with CuKα radiation at λ =1.5418 Å. Morphological studies and energy dispersive X-ray investigations have been performed with a Jeol JSM6360 high resolution scanning electron microscope (HR-SEM) equipped with energy dispersive X-ray analysis (EDX) for assimilating the elemental chemical analysis. UV-Visible diffuse reflectance spectrum (DRS) was recorded using Cary100 UV-Visible spectrophotometer to evaluate the energy band gap. The photoluminescence (PL) properties were recorded by using Varian Cary Eclipse fluorescence spectrophotometer. Magnetic measurements were performed at room temperature using PMC Micro Mag 3900 model vibrating sample magnetometer (VSM) equipped with 1 Tesla magnet.

Results and discussion

XRD analysis

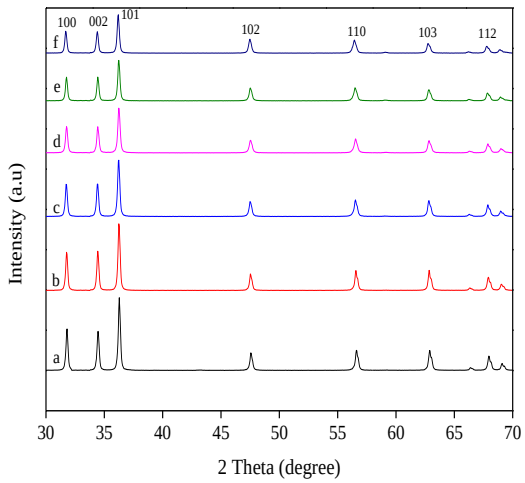

Figure 1. (a–f) XRD patterns of (a) pure ZnO, (b) $Zn_{0.98}Ce_{0.01}Mn_{0.01}O$, (c) $Zn_{0.96}Ce_{0.02}Mn_{0.02}O$, (d) $Zn_{0.94}Ce_{0.03}Mn_{0.03}O$, (e) $Zn_{0.92}Ce_{0.04}Mn_{0.04}O$, (f) $Zn_{0.90}Ce_{0.05}Mn_{0.05}O$ samples.

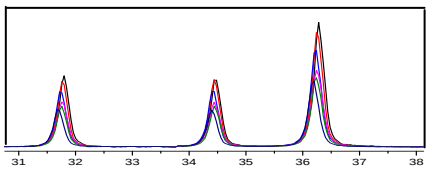

Figure 2. The centers of the three most intense peaks (100), (002), and (101)

The XRD patterns of the prepared ZnO and dual doped ZnO powders are displayed in Fig. 1. The sharp diffraction peaks prove that the as-prepared powders have high crystallinity. Fig. 1(a–f) illustrates that the typical diffraction peaks located at 2θ = 31.77°, 34.44°, 36.26°, 47.52°, 56.56°, 62.84°, 66.32°, 67.92°, and 69.03° correspond to (100), (002), (101), (102), (110), (103),(200), (112), (201), (004) and (202) reflections and it is in conformity with hexagonal wurtzite which matches well with JCPDS Card No. 89-0510. It is observed that the peak position is shifted to higher 2θ side and the peak intensity decreases simultaneously as shown in Fig.2. This fact is ascribed to the presence of co-dopants Ce, Mn in ZnO matrix, due to the difference in the ionic radii of Ce^{3+} and Mn^{2+} ions as compared to that of Zn^{2+}. The shift and decrease of intensity in XRD peaks with doping firmly suggest that Ce^{3+} and / Mn^{2+} ion successfully substituted into the ZnO host structure at the Zn^{2+} site. The formation of particles in the form of spheroids or spheres might be a clue that Ce, Mn has incorporated into ZnO matrix[7]. The average crystal size of the nanoparticles is estimated after appropriate background correction from X-ray line broadening of the diffraction peaks of (101) plane using Debye Scherrer's formula[8].

$$L = \frac{0.89\lambda}{\beta \cos\theta} \qquad (1)$$

where, L is the crystallite size, λ , the X-ray wavelength, θ, the Bragg diffraction angle and β, the full width at half maximum (FWHM). And the crystallite size is established to be 35.87, 36.09, 36.99, 37.06, and 37.96 nm respectively. The crystallite sizes of the samples are tabulated in Table 1. The size of the particles increased with the increase of (Ce, Mn) co-doping

Table 1. Crystallite size and band gap values of pure and dual doped samples

Samples	Crystallite size (nm)	Band gap (eV)
Pure ZnO	35.36	3.22
$Zn_{0.98}Ce_{0.01}Mn_{0.01}O$	35.87	3.19
$Zn_{0.96}Ce_{0.02}Mn_{0.02}O$	36.09	3.18
$Zn_{0.94}Ce_{0.03}Mn_{0.03}O$	36.99	3.16
$Zn_{0.92}Ce_{0.04}Mn_{0.04}O$	37.06	3.15
$Zn_{0.90}Ce_{0.05}Mn_{0.05}O$	37.96	3.12

3.2. Scanning electron microscopy (SEM) observations

Fig. 3 (a-d) shows the surface morphology of pure and dual doped ZnO nanoparticles. It has mixture of hexagon-like and spheroid-like particle structure with un-even grain size around 20 to 40 nm having better crystal quality. They are homogeneous and uniformly distributed throughout the structure. It is observed that the size of the particle get reduced and the particles are agglomerated with each other to have the grain size around 15 to 10 nm. The spheroid-like and hexagon-like structures of nanoparticles are turned into sphere like structures when co dopant concentration increases. From the above results, both the crystallite size and surface morphology are affected significantly by dual doping. When Ce and Mn were introduced into ZnO lattice, the grain size decreased continuously. The decreasing trend in the grain size with increasing dopant content shows that the dopants act as a grain growth inhibitor[9]. Besides, it has been noticed that the crystallite size and microstructure is altered by the nature and the size of the dopants. Therefore, SEM images exhibit that the surface morphology depends upon the concentration of dopants.

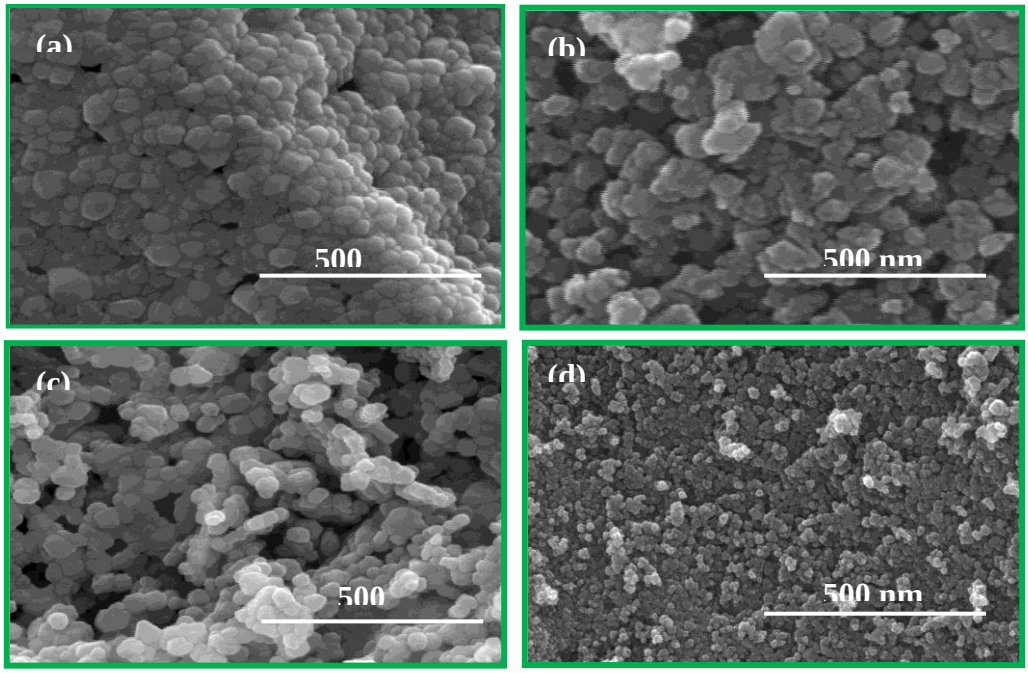

Figure 3. (a–d) HR-SEM images of (a) pure ZnO, (b) $Zn_{0.98}Ce_{0.01}$ $Mn_{0.01}O$, (c) $Zn_{0.94}Ce_{0.03}$ $Mn_{0.03}O$, (d) $Zn_{0.90}Ce_{0.05}$ $Mn_{0.05}O$ samples.

Energy dispersive X-ray (EDX) analysis

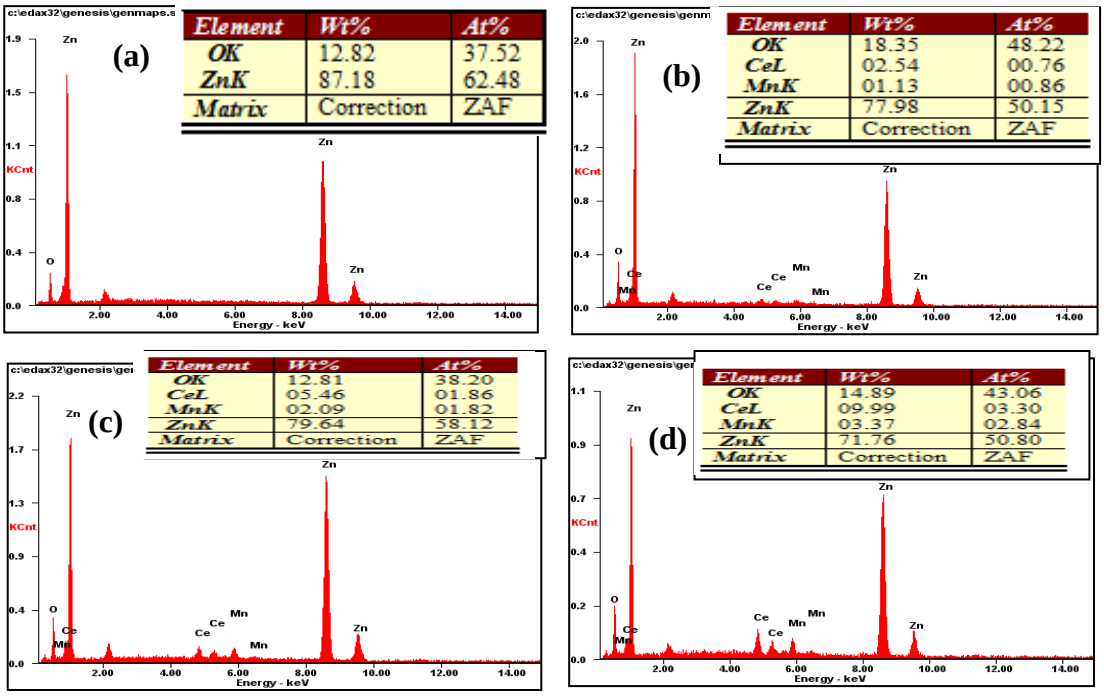

Figure 4. (a–d) EDX spectra of (a) pure ZnO, (b) $Zn_{0.98}Ce_{0.01}$ $Mn_{0.01}O$,(c) $Zn_{0.94}Ce_{0.03}$ $Mn_{0.03}O$, (d) $Zn_{0.90}Ce_{0.05}$ $Mn_{0.05}O$ samples. The inset table shows the quantitative weight and atomic percentage of the compositional elements.

The EDX spectra of the undoped and dual doped ZnO sample have been displayed in Fig. 4 (a-d). The EDX spectra performed on the dual doped ZnO nanostructures affirm the simultaneous presence of Zn, O, Ce and Mn. The absence of other elements in the EDX spectrum confirms the phase-purity and all the samples possess good stoichiometry in agreement with the chemical composition of the respective samples.

Optical properties (Diffuse Reflectance Spectroscopy)

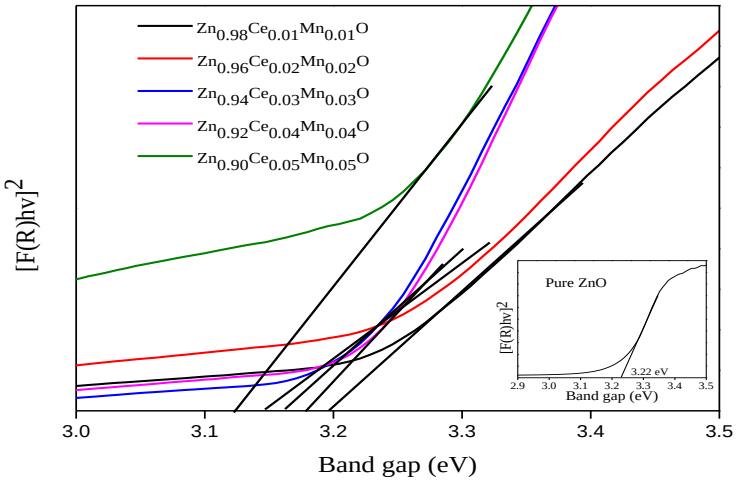

Figure 5. UV–Visible diffuse reflectance spectra of $Zn_{1-2x}Ce_x$ Mn_xO (x = 0.00, 0.01, 0.02, 0.03, 0.04 and 0.05) system. Inset figure UV–Visible diffuse reflectance spectra pure ZnO

The diffuse-reflectance analysis was performed on the samples in the UV–Vis region at room temperature. Fig. 5 shows the band gap energies of the Ce Mn dual doped ZnO samples, which were calculated from the diffuse-reflectance spectra using the Kubelka–Munk function[10] and the F(R) value is estimated from the following equation,

$$F(R) = (1-R)^2/2R \qquad (2)$$

F(R) is the Kubelka– Munk function, where R is the reflectance. A graph was plotted between $[F(R)h\upsilon]^2$ and hυ, the intercept value is the band gap energy as shown in Fig. 5. The determined values of the band gap of $(Zn_{1-2x}Ce_xMn_x)$ O (x = 0.00, 0.01, 0.02, 0.03, 0.04 and 0.05) system are 3.22, 3.19, 3.18, 3.16, 3.15 and 3.12 eV, respectively. The decline in the band gap also may be due to the s-d and p-d exchange, which give rise to the negative and positive corrections to the conduction and the valence band edges correspondingly, leading to the band gap narrowing[11].

Photoluminescence analysis (PL) study

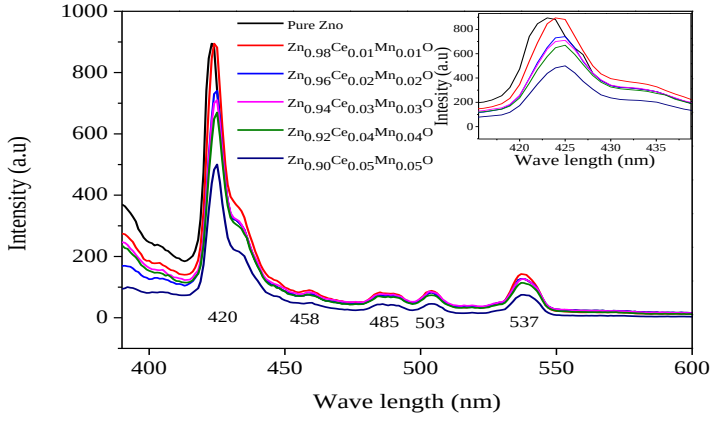

Figure 6. PL spectra of $Zn_{1-2x}Ce_x$ Mn_xO (x = 0.00, 0.01, 0.02, 0.03, 0.04 and 0.05) system. Inset figure shift in the peak at 420 nm.

Fig. 6 exhibits the room temperature PL spectra of the undoped and dual doped ZnO nanoparticles excited at 325 nm at room temperature. The PL spectrum for the as synthesized samples consists of a violet band centered at 420 nm, which may arise from the electron transition from shallow donor levels (Zn_i) to the valence band. The blue emission at 458 and 485 nm are assigned to the band-edge free excitons and bound

excitons[12]. The blue emission generates from the electron transition from the shallow donor level of oxygen vacancies to the VB and electron transition from the shallow donor level of zinc interstitials to the VB[13]. The green emission exhibited by the sample at 503 and 537 nm is related with oxygen vacancies and other vacancy related defects[14]. The broad PL band in the green region at 537 nm is traced to the defect levels associated with oxygen vacancies or zinc interstitial[15]. The reduction in the emission intensity with dual doping may be due to the increase in the nonradiative recombination processes[16]. It might be caused by the doped cations as they provide the competitive pathways for recombination, which results in the quenching of the emission intensity. The inset figure shows that the PL peak position of the dual doped samples shifts to the lower energies when compared to that of pure ZnO. The reason for this trend is that the band gap of dual doped samples is narrower than that of Pure ZnO. This result is in good agreement with the optical absorption spectra and shown in Fig. 5.

Magnetic (VSM) measurements

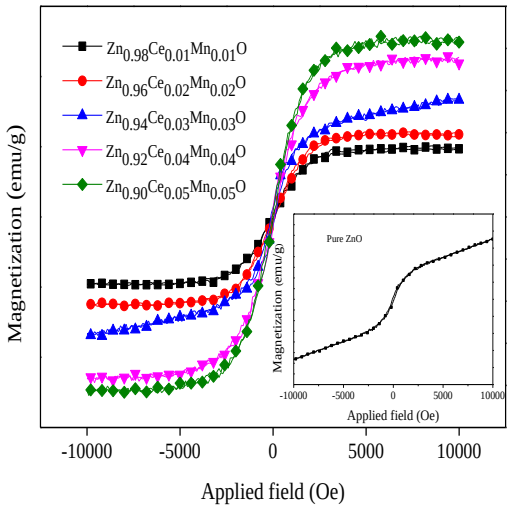

Figure 7. Magnetic hysteresis (M–H) loops of $Zn_{1-2x}Ce_x$ Mn $_xO$ (x = 0.00, 0.01, 0.02, 0.03, 0.04 and 0.05) system. Inset figure magnetic hysteresis (M–H) loops of pure ZnO

Fig. 7 displays the magnetization versus magnetic field (M–H) loops at room-temperature for ZnO, and dual doped ZnO samples. All the loops exhibit the relative magnetization with S-shaped hysteresis curves implying the presence of ferromagnetism. The coercive force of (($Zn_{1-2x}Ce_xMn_x$) O (x = 0.00, 0.01, 0.02, 0.03, 0.04 and 0.05)) samples were 68.82 Oe, 69.01 Oe, 72.01Oe 89.45 Oe 122.3 Oe and 158.1Oe, correspondingly. It can be seen from the Fig.7 that with an increase in the concentration of the doping ions, the saturation magnetic moment (Ms) is increased from 0.0059–0.0136 emu/g as shown in Table 2. The increases in magnetization in the highly Mn doped sample signify that Mn doping into ZnO induces ferromagnetism. Concerning the origin of the RTFM order in the samples, this may not be from the Mn-related secondary phases, because no trace of their presence was seen in the structural analysis. Several studies have explained the role of the secondary phase, connection between the defects and magnetism, and oxygen vacancy, etc.[17].

Table 2. Magnetization, remanance and coercivity of $Zn_{1-2x}Ce_xMn_xO$ (x = 0.00, 0.01, 0.02, 0.03, 0.04 and 0.05) system.

Samples	H_c(Oe)	M_r(emu/g)	M_s(emu/g)
Pure ZnO	68.82	2.2×10^{-4}	0.0057
$Zn_{0.98}Ce_{0.01}Mn_{0.01}O$	69.01	4.6×10^{-4}	0.0059
$Zn_{0.96}Ce_{0.02}Mn_{0.02}O$	72.65	1.3×10^{-4}	0.0082
$Zn_{0.94}Ce_{0.03}Mn_{0.03}O$	89.45	1.2×10^{-4}	0.0104
$Zn_{0.92}Ce_{0.04}Mn_{0.04}O$	122.3	1.1×10^{-4}	0.0124
$Zn_{0.90}Ce_{0.05}Mn_{0.05}O$	158.1	1.4×10^{-4}	0.0136

Summary and conclusion

Pure and dual doped ZnO nano particles with hexagonal crystal structure were prepared by the microwave combustion process and were characterized by XRD, SEM , EDX DRS, VSM, and PL. Results of XRD affirmed the wurtzite structure of the samples. At the same time, the shift in the peak, and increase in the crystallite size upon doping were also observed. SEM characterization results exposed that the obtained samples were nanoparticles with an average size of about 10 nm. The energy dispersive X-ray spectra confirmed the presence of Ce and Mn in ZnO system and the weight percentage was nearly equal to their nominal stoichiometry structure. DRS measurements reported a decrease in the energy gap with increasing dopants content. The PL results admit that the luminescence in the green, violet and blue regions strongly depends on the doping elements owing to the different oxygen vacancy, zinc interstitial, and surface morphology. Magnetic measurements demonstrate that the Mn ions doping concentrations play an important role in the ferromagnetic properties of Ce–Mn dual doped ZnO nanoparticles at room temperature.

References:

1. Hwang H.Y, Iwasa1Y, Kawasaki M, Keimer B, Nagaosa N, Emergent phenomena at oxide interfaces, Nat. Mater. 2012, 11; 103–113.
2. Wilson K.C, Manikandan E, Ahamed BM, Nanoflower rod wire-like structures of dual metal (Al and Cr) doped ZnO thin films: Structural, optical and electronic properties, Mater. Lett. 2014, 120; 295–298.
3. Zeng H, Duan G, Li Y, Yang S, Xu X, Cai W, Blue luminescence of ZnO nanoparticles based on non-equilibrium processes: defect origins and emission controls, Adv. Funct. Mater. 2010, 20; 561–572.
4. Fangli D, Ning W, Dongmei Z, Yingzhong S, Preparation, characterization and infrared emissivity study of Ce-doped ZnO films, J. Rare Earths 2010, 28; 391–395.
5. George A, Sharma S.K, Chawla S, Malik M.M, Qureshi M.S, Detailed of X-ray diffraction and photoluminescence studies of Ce doped ZnO nanocrystals, J. Alloys Compd. 2011, 509; 5942–5946.
6. Koseoglu Y, A simple microwave-assisted combustion synthesis and structural, optical and magnetic characterization of ZnO nanoplatelets, Ceram. Int. 2014, 40; 4673–4679.
7. Silva R, Zaniquelli M, Morphology of nanometric size particulate aluminium doped zinc oxide films, Colloid Surf. A 2002, 198; 551–558.
8. Kumar K, Chitkara M, Sandhu I.S, Mehta D, Kumar S, Photocatalytic, optical and magnetic properties of Fe-doped ZnO nanoparticles prepared by chemical route, J. Alloys Compd. 588 2014, 588; 681-689.
9. Murtza G, Iqbal M.A, Effect of Ho^{3+} substitutions on the structural and magnetic properties of $BaFe_{12}O_{19}$ hexaferrites, J. Alloys Compd. 2010, 495; 229-233.
10. Bruce, Hapke, Theory of Reflectance and Emittance Spectroscopy, University Press, Cambridge, 1993.
11. Wang R.C, Lin HY, Cu doped ZnO nanoparticle sheets, Mater. Chem. Phys. 2011, 125; 263–266.
12. Jing L, Qu Y, Wang B, Li S, Jiang B, Yang L, Fu W, Fu H, Sun J, Review of photoluminescence performance of nano-sized semiconductor materials and its relationships with photocatalytic activity, Sol. Energy Mater. Sol. Cells 2006, 90; 1773–1787.
13. Mariappan R, Ponnusamy V, Suresh P, Effect of doping concentration on the structural and optical properties of pure and tin doped zinc oxide thin films by nebulizer spray pyrolysis (NSP) technique, Superlattices Microstruct. 2012, 52; 500–513.
14. Wang X, Zhang Q, Wan Q, Dai G, Zhou C, Zou B, Controllable ZnO architectures by ethanolamine-assisted hydrothermal reaction for enhanced photocatalytic activity, J. Phys. Chem. C 2011, 115; 2769–2775.
15. Ding J, Yana X, Xue Q, Study on field emission and photoluminescence properties of ZnO/grapheme hybrids grown on Si substrates. Mat. Chem. Phys. 2012, 133; 405– 409.
16. Roy V.A.L, Djuri A.B, Liu H, Zhang X.X, Leung Y.H, Xie M.H, Gao J, Lui H.F, Surya C, Magnetic properties of Mn doped ZnO tetrapod structures, Appl. Phys. Lett. 2004, 84; 756–758.
17. Pearton S.J, Norton D.P, Ip K, Heo Y.W, Steiner T, Recent progress in processing and properties of ZnO, Prog. Mater. Sci. 2005, 50; 293–340.

*****